DESY PRC R&D 02/01
The Forward Calorimetry (FCAL) Group
Type of Document: Status Report

R & D for the TESLA-Detector: Instrumentation of the Very Forward Region

U. Druhakou[a], R. Ingbir[b], K. Kousnetzova[c], W. Lohmann[c], L. Suszycki[d] and W. Wierba[e], on behalf of the Forward Calorimetry group (FCAL)

[a] NC PHEP, Minsk, Belarus,[b] Tel-Aviv University, Tel-Aviv, Israel, [c] DESY, Zeuthen, Germany, [d] AGH University of Science and Technology, Cracow, Poland, [e] Institute of Nuclear Physics, Cracow, Poland.

26. October 2004

Wolfgang Lohmann, wlo@ifh.de

Abstract

The first two years of research work of the Forward Calorimetry (FCAL) Group are reviewed. Monte Carlo simulations to optimize the shape and segmentation of the calorimeters are done and a rough structure which matches the functionality is fixed for the calorimeters. For LumiCal the most critical parameters are identified and solutions to control them are under work. In the future simulations including realistic sensor design have to be done with very high statistics to verify the feasibility of the final goal. In parallel, the design of the mechanics, the silicon sensors and the alignment system is under way. The BeamCal simulations have shown the potential of the device for the physics program and for beam monitoring. The expected performance of a diamond-tungsten calorimeter is found to be superior. A third calorimeter, PhotoCal, is proposed to support beam monitoring. Sensors of three technologies for the innermost calorimeters are investigated. These are diamond sensors, heavy element crystals and a heavy gas ionization chamber. The results of all technologies are very promising

1 Introduction

The goal of the R&D program is to develop detector technologies for the instrumentation of the very forward region of a linear collider detector. The very forward region is a particularly challenging area for instrumentation. In the TESLA detector, two calorimeters, BeamCal (Beam Calorimeter) and LumiCal (Luminosity Calorimeter)[1] are planned. The BeamCal is positioned just adjacent to the beam-pipe in front of the final focus quadrupoles. It will be hit by beamstrahlung remnants giving a deposition of several tens of TeV per bunch crossing. The distribution of this energy will be measured to assist in tuning the beams. Single high energy electrons from e^+e^- scattering will be identified and measured. High energy electron identification is particularly important to veto backgrounds to new particle searches. Novel detector technologies need to be developed to fullfil the goals. Monte Carlo simulations are presented for a diamond/tungsten sandwich structure and compared to results obtained for a heavy element crystal calorimeter. First tests of sensors are described. A third calorimeter, PhotoCal, is proposed to measure the tails of the beamstrahlung photons downstream. The spectra of these photons are found to be sensitive to the actual beam parameters.

The LumiCal will measure larger polar angles than the BeamCal. It will provide a high precision ($O(10^{-4})$) luminosity measurement from Bhabha scattering. Monte Carlo simulations to optimize the shape and the structure of the calorimeter are presented. Part of the results reviewed here are published in Ref. [1].

2 The New Layout of the Forward Region

The maximal distance between the forward calorimeters BeamCal and LumiCal and the interaction region is determined mainly by the focal length L^* of the final focus system[2] . In the TESLA TDR [2] $L^* = 3$m was chosen, making the space for the forward calorimeters very limited. The structure proposed for the LumiCal on the tip of the tungsten mask was not compact and in front of the ECAL. Monte Carlo simulations of Bhabha events have shown that showers of electrons are not fully contained in the LumiCal, resulting in a deterioration of resolution in the polar angle and energy [3]. Furthermore, particles leaking the LumiCal would hit the ECAL end-caps. Due to the high rate of Bhabha events and the large distance between LumiCal and ECAL these particles would often be recognized as electromagnetic clusters in the ECAL. From the practical point of view signal readout and cabling are very difficult because of the extremely limited space behind the calorimeters.

Recently a new final focus system with a larger L^* values was considered [4]. The calorimeters could then be placed at larger distances from the interaction point behind the end-caps of the ECAL. Using $L^* = 4.15$ m a new design is proposed [5], as shown in Fig. 1. LumiCal is now a compact calorimeter with potentially much better performance and small leakage. In addition, radially space is forseen for the readout of the sensor planes in

[1]In the TESLA TDR these calorimeters are denoted as LCAL and LAT. Since these terms are not fully matching the functionality we changed them.

[2]The position of the quadrupole magnets of the final focus system limits the space along the beam-line.

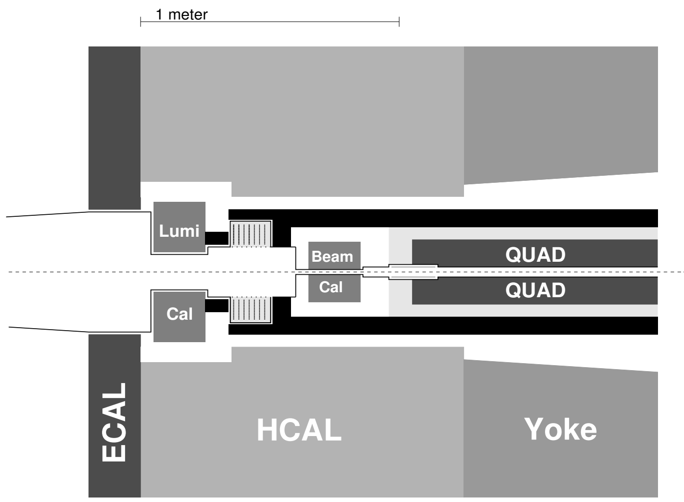

Figure 1: The two forward calorimeters BeamCal and LumiCal. The conical beam-pipe on the left points to the interaction region. The distance between the interaction point and the LumiCal is about 3 m. The BeamCal covers a polar angle range between 4 and 28 mrad and the LumiCal covers angles between 26 and 82 mrad. ECAL and HCAL are the electromagnetic and hadron calorimeters, respectively, and QUAD is the last quadrupole magnet of the beam delivery system. The multi-line vertical structure between LumiCal and BeamCal is a vacuum pump.

both calorimeters. Auxiliary electronics can be placed at the rear side of the calorimeters.

The particle flux backscattered from beamstrahlung interactions downstream in the beam-pipe is simulated and compared to the TDR design [6]. The occupancy induced in the silicon tracking devices and in the TPC are slightly more than for the TDR design but still uncritical.

3 Luminosity Measurement

LumiCal will be the luminometer of the linear collider detector. Furthermore, it will extend the coverage of the detector to polar angles of 26 mrad. The accuracy of the luminosity measurement is derived from the physics program. The GigaZ [2] program focuses on the measurement of fundamental parameters from the Z line-shape. In order to exploit the physics potential of GigaZ the uncertainty on the luminosity must be as small as $\sim 2 \times 10^{-4}$ [7]. Luminosity precision of better than 10^{-3} is necessary to study processes like $e^+e^- \to W^+W^-$ and $e^+e^- \to f\bar{f}$ at high energies. The cross section for $e^+e^- \to W^+W^-$ is strongly forward peaked where the forward peak is largely dominated by t-channel neutrino exchange. A precise luminosity measurement is needed to probe anomalous $e\nu W$ couplings. The process $e^+e^- \to f\bar{f}$ is sensitive to new physics at very high energy scales via interference with the Standard Model amplitude. To detect deviations from the Standard Model precise cross section measurements are necessary.

The luminosity measurement will be performed using the Bhabha process $e^+e^- \rightarrow e^+e^-(\gamma)$. At LEP, a systematic measurement uncertainty 3.4×10^{-4} was achieved [8], while the theoretical error was estimated to be 5.4×10^{-4}, updated recently to 4.5×10^{-4} [9]. The major contributions to this uncertainty are the uncertainty of $\alpha(q^2)$, two-loop virtual corrections and direct pair production.

Several efforts to reach a 10^{-4} precision in the theoretical cross section calculations are undertaken. The MC program BHLUMI [10], which was successfully used at LEP experiments, is being upgraded to an improved version based on a completely new cellular algorithm FOAM [11]. Independently, the MC generator SAMBHA was developed [12]. Large projects to calculate the contributions from the 2-loop virtual QED and 1-loop EW corrections, with corresponding bremsstrahlung, to Bhabha scattering have started at DESY (Zeuthen) and University of Katowice [13] and at the Universities of Bologna and Freiburg [14].

The Bhabha process also offers the possibility to determine of the running of the electromagnetic coupling α. The knowledge of $\alpha(q^2)$ is important, because its current uncertainty limits the accuracy of the prediction of the electroweak quantities within the Standard Model, e.g. the prediction of the Higgs mass. The measurement of the difference $\alpha(t_{min}) - \alpha(t_{max})$, where for small scattering angles $t \approx -(E_b \cdot \theta)^2$, would improve the knowledge of $\alpha(q^2)$. At GigaZ the running of α above $t = (1.2\text{GeV})^2$ can be probed. This q^2 range corresponds to a region where precise cross section measurements of the process $e^+e^- \rightarrow$ hadrons are not yet done.

3.1 Monte Carlo Simulations of LumiCal

The LumiCal covers polar angles θ between 26 and 82 mrad. Two versions of a silicon-tungsten calorimeter are simulated. In the first version (pad), the silicon sensor plane is subdivided radially into rings and azimuthally into sectors, forming readout pads. Longitudinally the calorimeter is composed of layers, each layer consisting of a tungsten absorber disk and a sensor plane. The energy deposited on each pad is read out. The thickness of the tungsten layer is one radiation length and the gap for sensors is chosen to be 4 mm. The sensor thickness is 0.5 mm. In the standard pad version each sensor plane is subdivided into 15 rings and 24 sectors. In the second version (strip), the absorber structure is similar. The sensor planes alternate between sensors with 64 concentric strips and sensors with 120 radial sectors. Sensors of 0.5 mm thickness are glued on a ceramic carrier of 1.5 mm thickness. For bonds and signal readout 1 mm additional space is left between the tungsten disks. In depth both calorimeters are composed of 30 layers.

The detector simulation is done using the BRAHMS [15] package which is based on the Geant 3.21 [16] detector simulation program. Bhabha scattering events are generated with the BHLUMI [10] and BHWIDE [17] packages. The program CIRCE [18] is used to include beamstrahlung losses. In addition, Gaussian beamspread is applied, using values for the width of $0.05\%\sqrt{s}$ and $0.5\%\sqrt{s}$, respectively. The distribution of the energy carried by the final state $\mathrm{e}^+\mathrm{e}^-$ pair for a centre-of-mass energy of 500 GeV is shown in Fig. 2.

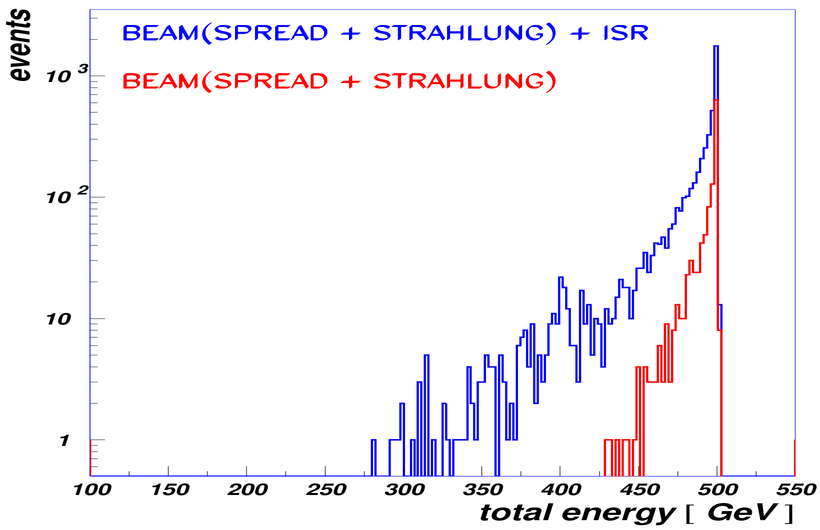

Figure 2: The distribution of the energy carried by the electron and positron using BH-WIDE and CIRCE packages. The centre-of-mass energy is 500 GeV and a beam spread of $0.05\%\sqrt{s}$ is applied. The red histogram includes beamstrahlung, the blue one beam-strahlung and initial state radiation.

3.1.1 Resolution Studies

The position of the showers in both versions is reconstructed from the energy depositions on the sensors pads or strips using a weight function:

$$< x >= \frac{\sum_i x_i W_i}{\sum_i W_i}. \tag{1}$$

Only significant depositions are considered introducing the following logarithmic weight function [19]:

$$W_i = \max\{0, [C + \ln \frac{E_i}{E_{Total}}]\}. \tag{2}$$

The constant C is determined by an optimization process under two criteria- best resolution and minimum bias. Using the logarithmic weighting, the resolution in the polar angle θ is improved, in comparison to a simple 'center of gravity' weighting, by a factor of about three. A systematic study revealed that the constant C is dependent on the beam energy, as shown in Fig. 3. The energy resolution is obtained from a Gaussian fit of the reconstructed shower energy distribution. It can be parametrised as in $\Delta E/E = 0.25/\sqrt{E}$ for the pad version and $\Delta E/E = 0.31/\sqrt{E}$ for the strip version of the calorimeter. The resolution in the polar angle θ was studied for single electrons and for Bhabha events including radiation and beam spread. The result for the pad version, $\sigma(\theta)$ as function of the beam energy, is

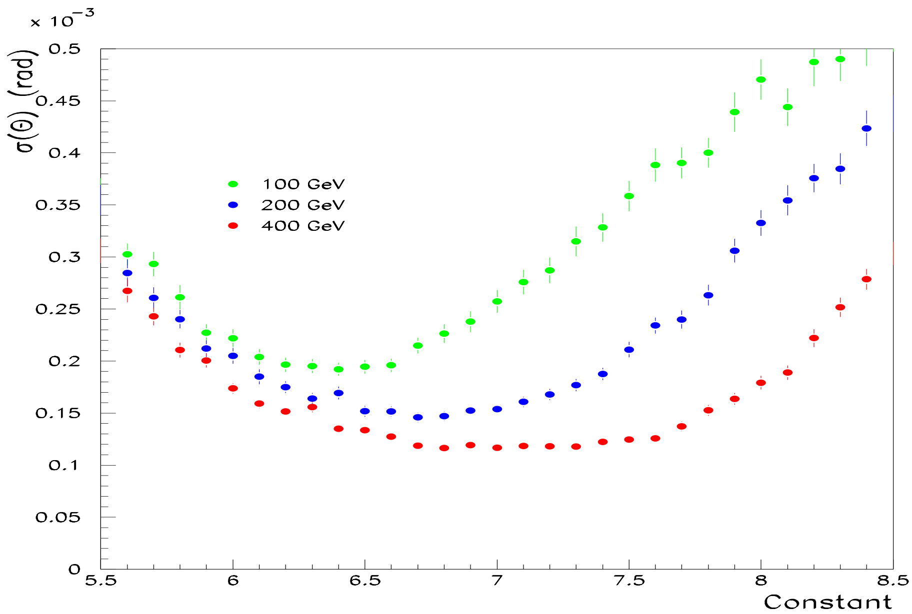

Figure 3: The resolution in the polar angle θ, $\sigma(\theta)$, as a function of the constant C used in the logarithmic weighting for beam energies of 100, 200 and 400 GeV. The pad version of the calorimeter is simulated.

shown in Fig. 4. Taking the θ resolution for the case of single electrons as a benchmark, the simulation of full Bhabha events and the beam spread affect the resolution only by a few per cent. At 250 GeV beam energy we expect a resolution of 1.5 $\times 10^{-4}$ rad. The remaining bias in the θ reconstruction is $\Delta\theta = 1.5 * 10^{-5}$ rad. In the strip design the polar angle resolution is $4 * 10^{-5}$ rad for the 250 GeV beam energy. This, in comparison to the pad version, much better value is due to the finer θ segmentation and the more compact structure of the strip version and should be regarded as the ideal benchmark resolution. A bias in the reconstructed azimuthal angle ϕ is caused by the magnetic field in the inner part of the detector. Choosing a 4 Tesla magnetic field the position of an electron of 250 GeV is shifted by about 8 mrad for polar angles around the center of the detector.

3.1.2 Event Selection for the Luminosity Determination

Showers near the inner and outer radius of the calorimeter are not fully contained. Hence, an acceptance cut in the polar angle θ is applied to reject these events.

The quantity needed for the luminosity calculation is the number of Bhabha events in a certain polar angle range. Due to the steep fall off of the Bhabha cross section as a function of θ the definition of the inner radius of the acceptance region is critical for the luminosity accuracy [20]. One possibility is to apply the acceptance cut on the measured θ angle of the reconstructed shower position. In that case all sensor layers must be precisely aligned and the bias in θ must be controlled. A second possibility is to use the energy deposited

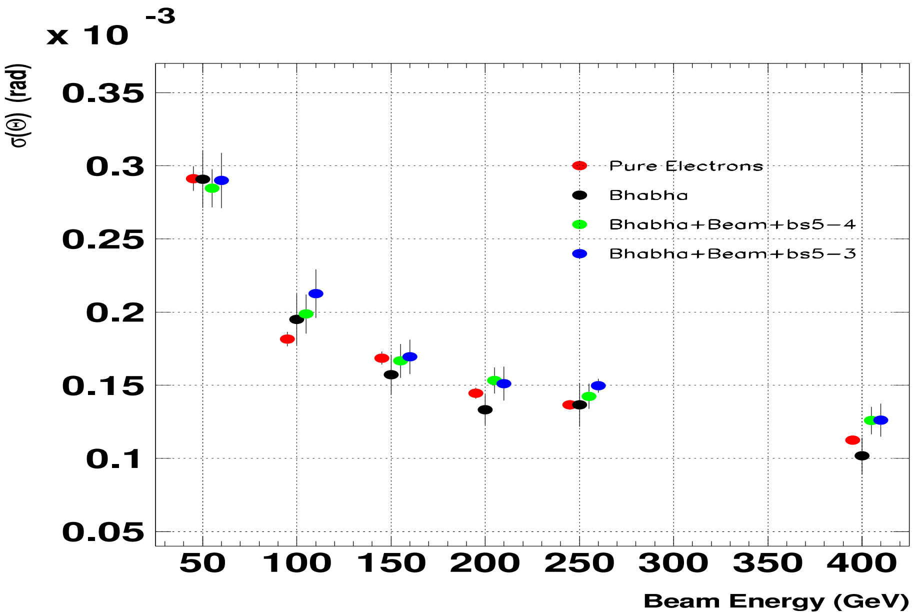

Figure 4: The resolution of the polar angle, $\sigma(\theta)$ as a function of the beam energy for single electrons (red), electrons from Bhabha generators (black), electrons from Bhabha generators with beamspreads of $0.05\%\sqrt{s}$ (green) and $0.5\%\sqrt{s}$ (blue) .

onto a few precision sensor layers in the center of the shower. The sharing of the deposited energy between two precision rings of pads is used to to decide whether an event is inside or outside the acceptance region. Applying loose selection cuts on the energy balance and acolinearity of the event, the distribution of the cut quantity using three precision layers is shown in Fig. 5. Due to the sharp step-function behavior this method seems to be very promising for the definition of the acceptance region. A high statistics Monte Carlo is in preparation to estimate its potential accuracy for Bhabha event counting.

3.1.3 Design Optimization

An attempt is made to change the detector parameters to further optimize the performance. The detector density was enhanced by increasing the thickness of the tungsten disks at expense of the gap foreseen for the sensors. This leads to a smaller Moliere radius and more radiation lengths. To maintain the θ resolution a finer sensor segmentation would be necessary resulting in a larger number of readout channels. The energy resolution becomes worse. Since the sensor layers at the rare end do not contribute to the resolution the detector would need less space along the beam. Optimization studies have also been made by changing the number of sectors. Increasing the number of sectors improves the ϕ resolution but does not affect the polar angle resolution.

To approach a realistic design for the sensor planes the effect of pad margins is studied. An extreme scenario is assumed in which around every pad there will be a dead sensor

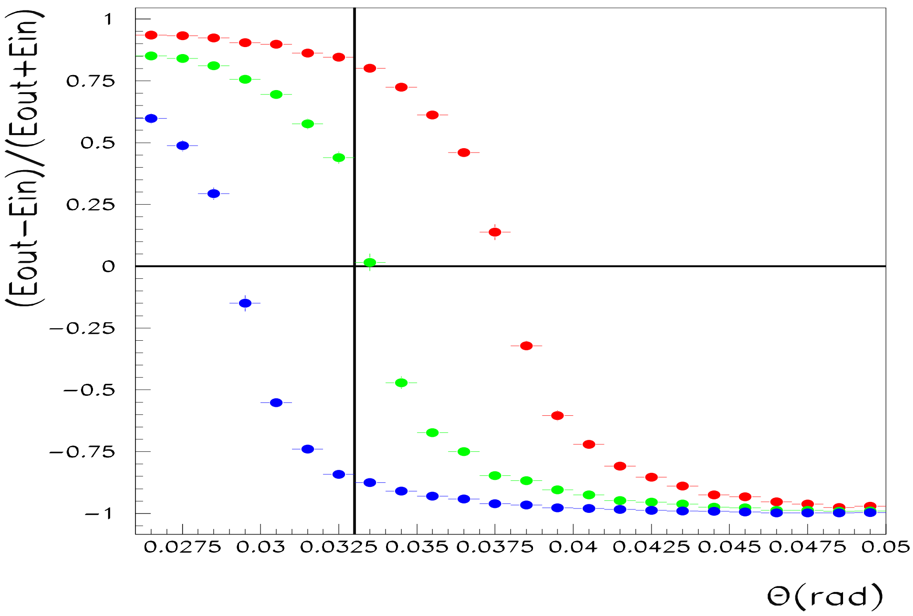

Figure 5: The normalized difference of energies deposited on the rings defining the inner acceptance region. The curves correspond to one (blue), two (green) and three (red) sensor pad rings, corresponding different θ_{min} values.

area. The detector performance studies repeated for different margin sizes. Up to margin sizes of 10 μm no change in the performance is observed.

A 'shower peak design' is defined where sensors around the shower maximum have a finer granularity as the sensors near the front and rear end of the calorimeter. Choosing for the first 4 layers 24 radial sectors and 10 rings and the next 15 layers 24 radial sectors and 22 rings and for the rear 11 layers the same segmentation as for the first 4 layers, the resolution in θ is improved by about 20% keeping the other parameters at the same values. The number of electronic channels is the same as in the standard design.

3.2 Proposal for the Mechanics Design, the Design of Sensors and Readout Electronics

3.2.1 Mechanical Structure

The two LumiCal versions are composed of segmented silicon sensors interspersed into the tungsten disks. The thickness of the tungsten is one radiation length (3.4 mm) and the gap for silicon sensors is a few mm[3]. A possible mechanical design in shown in Fig. 6. The calorimeter consists of two half barrels to allow for mounting on a closed beam pipe. The heavy part, the tungsten half disks, are supported by the blue bolts. The accuracy requirements for this frame are moderate.

[3] The minimal space needed for the sensor layers using current sensor assembly technologies is 3.1 mm.

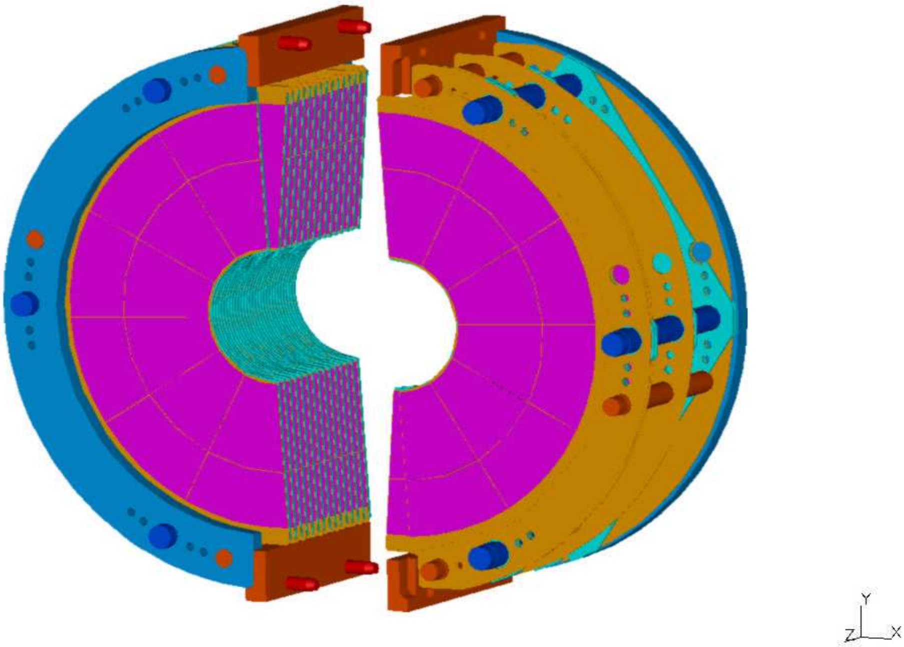

Figure 6: The mechanical structure of the LumiCal. The blue bolts support the tungsten disks. The red bolts form a precision frame to position the sensor layers. Holes in the support ring are forseen to allow a precise optical survey after the calorimeter is mounted.

The red bolts carry only the sensor half layers. This frame is decoupled from the tungsten disk support, hence it does not suffer by gravitational sag due to the heavy tungsten disks. The silicon sensors of 300 μm thickness are glued on a 1 mm thick ceramic support. Some space is left for bonding. The frame of the red bolts has to fulfill the extreme precision requirements for the sensor positioning. In order to be able to survey the precision layers in the center of the device after mounting, the support ring contains holes. The precision of the optical survey must be in the μm range. The design and test of such a survey system, including thermal stability, will be part of the proposal update. The positions of two half-barrels with respect to each other will be fixed through precise pins mounted at the top and bottom of each C shaped steel frame. The latter stabilizes the whole structure.

3.2.2 Alignment and Position Monitoring

The luminosity measurement requires precise alignment of the two LumiCal detectors to each other and precise positioning with respect to the beam-line and the interaction point. The beam pipe is proposed as a suitable reference. Also the Beam Position Monitors are mounted at fixed positions inside the vacuum pipe. This would allow to determine the actual LumiCal position with respect to the beam position. Monte Carlo simulations have shown [20] that the inner radius of the precision sensor layers must be known to the 1 μm level, the accuracy in the the transversal (x, y) displacement with respect to the beam is required to be known to 100 μm accuracy, and the distance between the two calorimeters along the beam axis must be known to an accuracy of 60 μm. The position monitoring should not interfere with the mechanical support of the detector, hence an optical system is preferred. We plan a laser system with a CCD matrix sensor to measure the transversal displacement of the LumiCal detector with respect to the beam pipe flange. A fine pixel CCD matrix offers X-Y measurements in a single position detector. Pixel size can be 5 μm $\times$ 5 μm on the 7 mm$\times$ 7 mm matrix. The laser beam spot will have the diameter of about 100-300 μm. We have proven that using a simple, low cost web camera with a resolution of 640x480 pixels connected to a computer via the USB port can achieve an accuracy of measuring the detector displacement to a few μm [21].

There are several issues that should be addressed to future R&D: The dependence of the accuracy on the pixel size, the optimal laser spot size, the methods to determine the center of the spot, saturation effects and the dependence on the laser wavelength. The use of a semiconductor diode laser or a diode pumped solid-state laser is considered for this purpose. These lasers are small in size, have a long lifetime, and the wavelength is well matched to the detector sensitivity characteristics. The angular stability of the laser beam pointing (micro pointing stability) has to be taken into account. The micro pointing stability is lower for this type of lasers compared to gas lasers (e.g. He-Ne). It is also possible to use a laser positioned outside the central area and to distribute the laser light via optical fiber. Exposure and readout synchronization in time slots between the trains of e^+ e^- beams should be carefully investigated to avoid background. The radiation hardness of the CCD sensor and of the electronics must be studied. The CCD sensor will be placed between the rear side of the LumiCal calorimeter and the tungsten shield. The radiation dose in that area probably will not be extremely high. The use of twin lasers in parallel configuration is considered. The detector size easily allows for that and the algorithms can cope with two laser spots. Such a configuration assures better reliability in case of a laser failure.

3.2.3 Silicon Sensors

The proposed segmentation of the silicon sensors for the best expected performance is: the first 4 layers will consist of 24 radial sectors and 10 rings, the next 15 layers, where the maximum of the shower is expected, will consist of 24 radial sectors and 22 rings, and the rear 11 layers will be segmented as the first 4 layers ('shower peak design'). The sensitive region extends from 80 mm to 260 mm in radius. The geometry of the diode for one sector is shown in detail in Fig. 7. for the rough (left) and the finer (right) segmentations. A single pad will have a radial pitch of 19.95 mm or 9.07 mm, respectively, and spans an angle of 15^0. Each sector will be built from two tiles of silicon sensors. This is necessary, because the current technology is based on 6-inch wafers. One may expect 8-inch wafer technology within next years, resulting in a similar tile subdivision. To produce the silicon sensors on one wafer, we would need 12-inch wafers. At the moment it is unclear whether such wafers will be available in future. The silicon sensor tiles will be glued to a thick film ceramic plate supporting 6 sectors of the half-barrel. Readout chips are placed radially outside the detector. We assume a 0.5 mm gap between the tiles and the sectors.

For the 'strip' version the odd layers contain 64 concentric strips with a radial pitch of 3.13 mm and the even layers 120 radial strips of 3°. The layout of both layers is shown in Fig. 8. The silicon pad or strip diodes will be usual planar silicon sensors. Reference marks are foreseen on the detector surface for precision positioning.

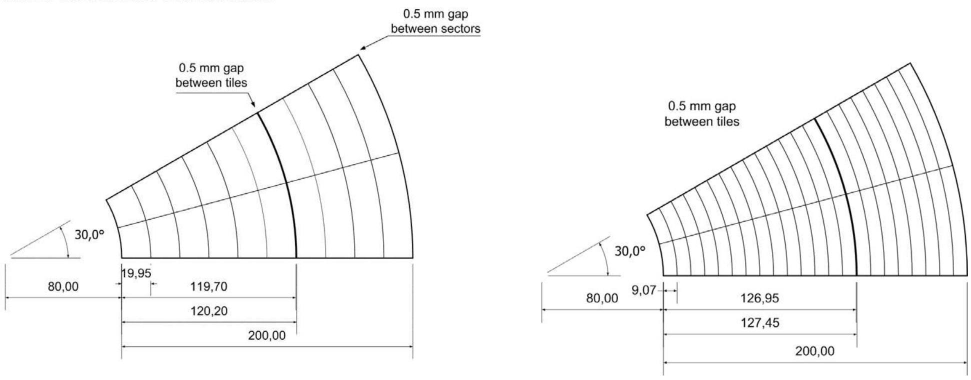

Figure 7: The layout of a silicon sensor sector of the pad version. On the left is the rough segmentation and on the right the fine segmentation of the 'shower peak design'.

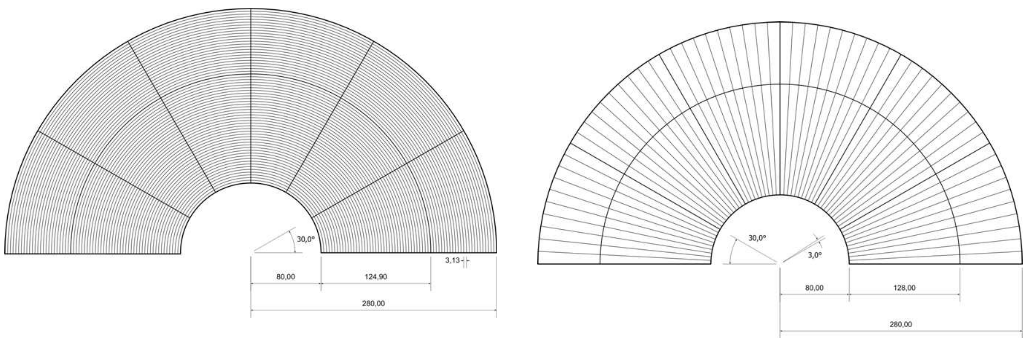

Figure 8: The layout of the silicon sensors of the trip version. The odd sensor layers contain concentric strips (left) and the even layers radial strips (right).

3.2.4 Electronics

The LumiCal electronics, especially the preamplifiers, must be carefully designed taking into account performance to be obtained from the more detailed MC simulations, limited space for electronics in the very forward region and acceptable heat dissipation. The large amount of readout channels favors the integration of the preamplifiers with the detector. We expect 11520 readout channels for the silicon pad version and 15120 channels for the strip version. Connection from each pad or strip to the preamplifier can be made using a Kapton flexfoil, a second metal layer with traces on the silicon surface or metal traces on the ceramic support plate. To ensure minimal cross talk from signals in adjacent sensors Kapton flexfoil or traces on ceramics are preferred. The 0.5 mm gap between tiles are wide enough for bonding the pads or strips to traces on the ceramic support plate. On a sensor half-plane up to 264 channels of the readout electronics should be placed, requiring highly-integrated chips. Technology options are radiation hard CMOS or bipolar preamplifiers. The proper technology will be worked out in close collaboration with other sub-detector groups to find a standard solution.

3.3 Previous Milestones for LumiCal

Most of the milestones concerning MC simulations are matched. An exception is the study of background processes. Here a study of beamstrahlung remnants is done. It is found that beamstrahlung remnants will not influence the LumiCal performance. Other background sources, e.g. two photon events, have not been considered so far and are part of the future work. From the milestones of hardware developments only studies of the laser alignment system are done [21]. Sensor prototyping reached the level of design, but basically no prototyping is done. Here more effort has to be invested in future.

4 The BeamCal

The BeamCal covers a polar angle range between 4 and 28 mrad. This angular region is strongly affected by electrons and positrons originating from beamstrahlung photon conversions. As discussed below, the energy density distribution depends on the beam parameters and will be measured to tune the beam for maximum luminosity. In addition, high energy electrons from two-photon processes have to be measured or at least vetoed to angles as close as possible to the beam. The latter is important since these events are a serious background in many search channels with missing energy and momentum [22]. The calorimeter also has to shield the central part of the detector against backscattered particles, induced by beamstrahlung remnants downstream in the beam-line, and synchrotron radiation[4]. The depositions of beamstrahlung remnants in the BeamCal result in an integrated radiation dose of up to 10 MGy/year for sensors near the beampipe [5]. Hence radiation hard sensors must be used.

[4]The amount of backscattered particles and synchrotron radiation is small in comparison to the beamstrahlung. However, the occupancy in the central detector would increase without the shielding provided by the BeamCal.

[5]The integrated dose is obtained using a realistic beam simulation, as explained later in this article.

4.1 Potential Technologies for BeamCal

Fine granularity is necessary to identify the localized depositions from high energy electrons and photons on top of the broader spread of energy from beamstrahlung remnants. The transverse granularity should be slightly less than a Molière radius. The signal from a high energy electron will then be concentrated in a few sensor segments on top of the background from beamstrahlung. Sharing the shower signal between neighboring segments will improve the position resolution. Since the beamstrahlung energy deposition varies considerably with R and ϕ and depends on the actual beam parameters, a dynamic range of $O(10^3)$ is required.

4.1.1 Silicon-Tungsten or Diamond-Tungsten Sandwich Calorimeter

Silicon-tungsten calorimeters were successfully used in LEP experiments [23]. The Molière radius can be kept to about a centimeter, leading to narrow showers for high energy electrons. A possible structure of the calorimeter is sketched in Fig. 9. It consists of two half-barrels placed just outside the beampipe. Diamond or silicon sensors (black) are

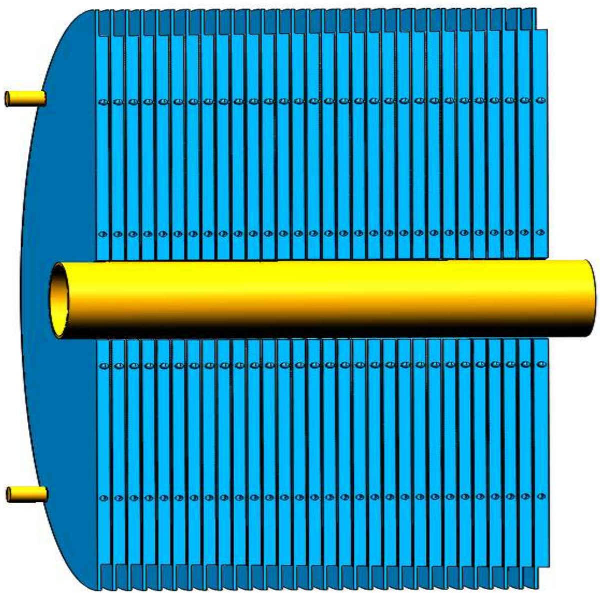

Figure 9: Drawing of the structure of a half barrel of the sandwich calorimeter. For the simulation described below the outer radius and the length along the beampipe are 10 cm and 12 cm, respectively. Sensors (black) are interspersed between tungsten disks (blue). The thickness of the tungsten absorber disks is one radiation length, the space for the sensor is 500 μm.

interspersed between tungsten disks (blue). The thickness of the tungsten disks is chosen to be one radiation length and the gaps for the sensors are 500 μm.

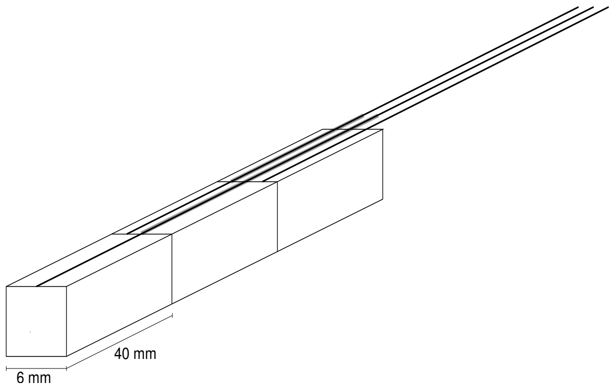

Figure 10: Scintillator pieces forming a segment of the crystal calorimeter. Each piece is connected to an optical fiber of 1 mm diameter which is optically isolated from the other pieces adjacent to the rear end of the calorimeter.

Studies of the radiation hardness of diamond sensors under electromagnetic radiation [24] have shown that doses up to 10 MGy do not influence the response to ionizing particles.

4.1.2 Crystal Calorimeter with Fiber Readout

A homogeneous crystal calorimeter promised better energy and time resolution than a sandwich calorimeter. As an example, we consider $PbWO_4$ as a scintillator with a Molière Radius of 2.2 cm. Longitudinal segmentation is obtained by cutting the crystals into pieces. Each piece of a calorimeter segment, as sketched in Fig. 10, is readout by an optical fiber. The fibers are routed to the back of the calorimeter into an area of low activity through grooves in the adjacent rear pieces. The fibers are painted black in these areas to prevent light from coupling into the routed fibers. Each scintillator piece is individually wrapped in a layer of Tyvek paper. Light from the fibers can be read out by multichannel photo-tubes or diodes.

An alternative readout technique has been proposed, using thin vacuum photodiodes with segmented anodes between each layer of crystals [25].

4.2 BeamCal Simulations

The BeamCal will be hit by the electrons and positrons originating from beamstrahlung photon conversion, carrying over 20 TeV of energy per bunch crossing (BX) [2]. The distribution of this energy is shown in Fig. 11. The energy density drops rapidly with growing radius. A sharp cutoff of the depositions is found at a radius of about 5 cm. However, a few particles can be found at larger radii. In the $r-\varphi$ plane, a strong variations with φ is found. The maximum energy density occurs at the top ($\varphi \approx 90^\circ$) and the bottom ($\varphi \approx 270^\circ$) region near the beam pipe. These result from the flat beams at the IP generating the bulk of the pairs in horizontal plane which then curl up in the magnetic field along the beam line.

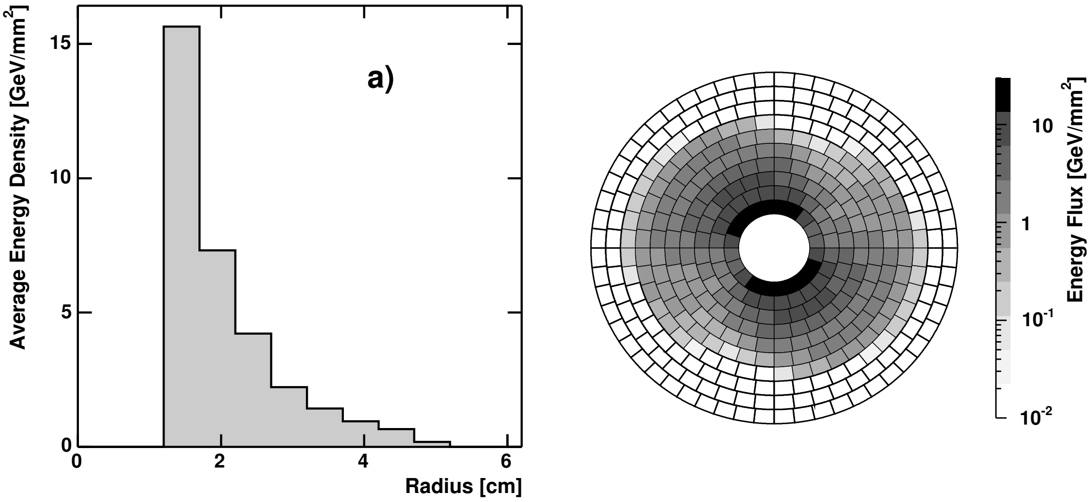

Figure 11: The energy density of beamstrahlung remnants per bunch crossing as a function of a) radius and b) (right) position in the $r-\varphi$ plane. The centre-of-mass energy is 500 GeV. The maximal value of the density is 30 GeV/mm^2.

High energy electron identification is particularly important to veto backgrounds to new particle searches [22]. Single high energy electrons should be thus identified on top of the beamstrahlung remnants depositions. The latter are hereafter denoted as background.

The reconstruction efficiency of single electrons is studied for the diamond-tungsten sandwich calorimeter and the crystal calorimeter. The simulations are done for 500 GeV centre-of-mass energy for TESLA standard beam parameters [26].

The background and single electrons are generated and tracked through the detector. Energy depositions from the background and single electrons in the sensor pads are superimposed and a reconstruction algorithm is applied to the output. The beamstrahlung is generated using GUINEA-PIG [27]. The GEANT3 [16] based detector simulation program BRAHMS [15] is used for the detector simulation.

4.2.1 Diamond Tungsten Sandwich Calorimeter

The simulated sampling calorimeter is longitudinally divided into 30 disks of tungsten, each 1 X_0 thick (3.5 mm) interleaved by diamond active layers (0.5 mm). The sensitive planes are divided into pads with a size of about half a Molière Radius (5 mm) in both dimensions, as shown in Fig.11b.

The efficiency to detect electrons is shown in Fig. 12 for several electron energies for regions with relatively low ($\varphi \approx 0°$) and high background ($\varphi \approx 90°$). An electron of 250 GeV is detected even in regions with high background with almost 100% efficiency. The efficiency drops near the innermost radius, partly due to shower leakage. Electrons of 50

GeV are identified with high efficiency only at larger radii.

The rate of fake electrons in e^+e^- annihilation events is estimated by applying the reconstruction algorithm to pure background events. Fake electrons may origin either from the tail of high energetic particles in beamstrahlung remnants or from background fluctuations which mimic an electron signal. In this study the reconstruction algorithm is tuned such that the rate of fake electrons with energies above 50 GeV is less than a per cent.

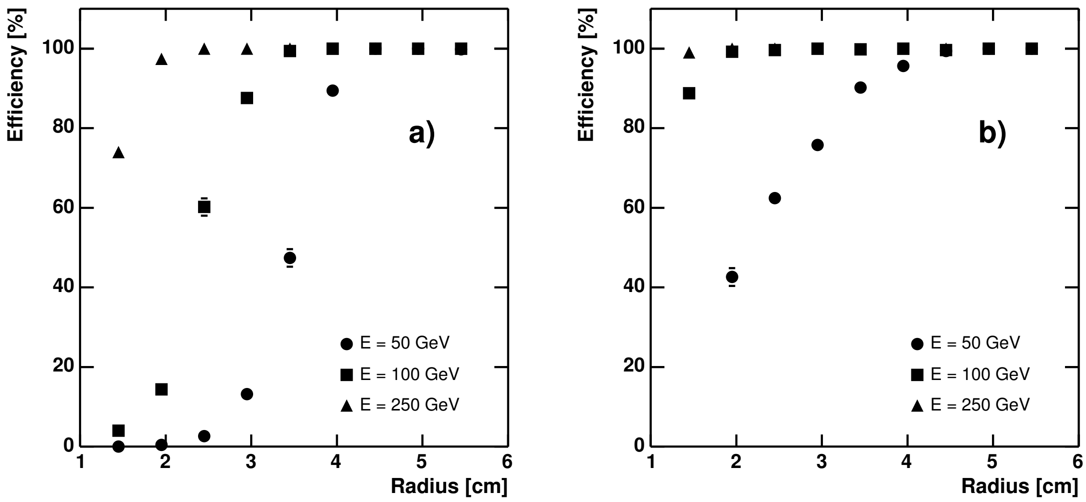

Figure 12: The efficiency to detect an electron of energy 50, 100, 250 GeV as a function of the radius a) at $\varphi \approx 90°$ and b) at $\varphi \approx 0°$ in the sampling calorimeter.

4.2.2 The $PbWO_4$ Crystal Calorimeter

Similar investigations are done with a heavy element crystal calorimeter. We consider $PbWO_4$ as a scintillator with a Molière Radius of 22 mm. The calorimeter segments, as shown in Fig. 10, are longitudinally divided into three pieces: 3 X_0 for the front piece, 9 X_0 for the middle and 8 X_0 for the rear piece. In this study the number of longitudinal pieces is minimized and their relative length is optimized to maintain high efficiency but keeping the fake rate to be less then a per cent. The first short piece does not contribute in the electron detection but is supposed to be used for analysis of the beamstrahlung remnants distribution in order to assist in beam diagnostics. The segmentation in the $r - \varphi$ plane is again about half of the Molière radius.

The efficiency to detect a 100 GeV electron as a function of the radius at $\varphi \approx 0°$ is shown in Fig. 13 and compared with the result from the sampling calorimeter. The performance of the sampling calorimeter is superior. A finer longitudinal granularity does not change the situation. A larger number of pieces will result in larger relative amount of fibres and wrapping material and reduce thus the volume filled with heavy crystals. The transverse shower shape is distorted and the shower leakage becomes larger.

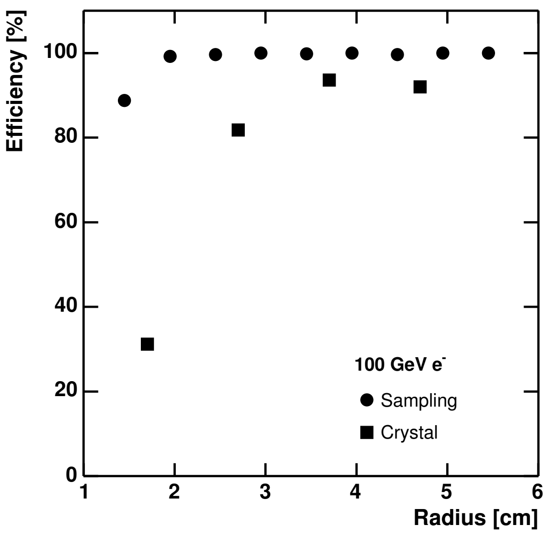

Figure 13: The efficiency to detect a 100 GeV electron as a function of the radius in the low background region for a crystal (squares) and sampling (dots) calorimeter.

4.2.3 The Effect of Realistic Beams

The studies for the sandwich calorimeter reported above are done for a situation called "ideal beam", since fluctuations caused by instabilities of the linear collider are neglected. The studies are repeated for a more realistic beam simulation which includes beam transport through the linac including wakefield effects, beam transport through the BDS including ground motion effects in the quadrupoles, and operation of a beam-feedback system adjusting the beams at the IP. The simulated beamstrahlung data files are provided by courtesy of Glen White [28].

Fig. 14 shows the average energy deposited on a pad near the beam pipe, and the corresponding rms, for sets of 10 successive bunch crossings sampled at the start of a TESLA bunch train. The total energy deposited in BeamCal can be larger for the more realistic simulation. However, the rms of energy depositions from a sequence of bunch crossings is similar to the ideal case, apart from a few bunch crossings at the beginning of the bunch train.

The efficiencies for the detection of high energy electrons for realistic and ideal beam simulations are compared in Fig. 15. The realistic beam treatment does not deteriorate the detection efficiency. The fake electron rate for realistic beam simulation is at the same level as for ideal beam.

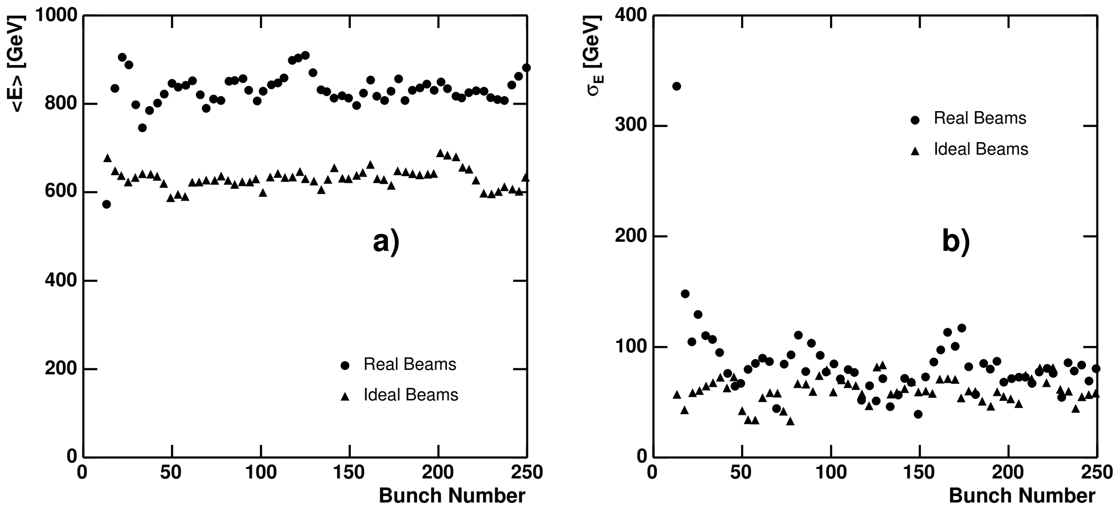

Figure 14: The energy deposited in one pad averaged over 10 bunch crossings a) and the corresponding rms of the energy b) for realistic (dots) and ideal (triangles) beam simulations. The quantities are shown for a sensor pad near the beam-pipe at $\varphi \approx 90^\circ$ as a function of the bunch number for the first 250 bunch crossings.

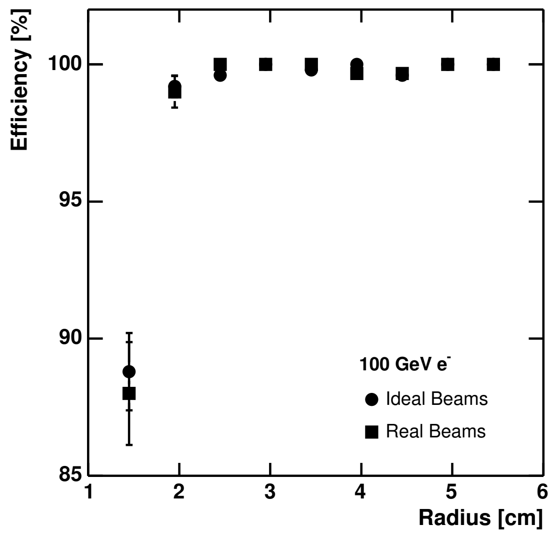

Figure 15: The efficiency to detect a 100 GeV electron as a function of the radius in the low background region for realistic (squares) and ideal (dots) beam simulation.

4.2.4 The Results for $\sqrt{s} = 1$ TeV

The studies for the sandwich calorimeter are repeated for 1 TeV centre-of-mass energy. Standard 800 GeV TESLA beam parameters [26] are assumed for 1 TeV. Some important beam parameters are given in Tab. 1. The comparison of the energy density distribution

$\sqrt{s}$ [GeV]	500	1000
Bunch charge [10^{10}]	2	1.4
$\gamma\epsilon_x$ / $\gamma\epsilon_y$ [mrad $\times$ 10^{-6}]	10 / 0.03	8 / 0.015
β_x / β_y [mm]	15 / 0.40	15 / 0.40
σ_x / σ_y [nm]	554 / 5.0	350 / 2.5
σ_z [μm]	300	

Table 1: TESLA beam parameters for centre-of-mass energies of 500 GeV and 1 TeV

at $\sqrt{s} = 1$ TeV, shown in Fig. 16, with the result at $\sqrt{s} = 500$ GeV (Fig. 11b) shows that beamstrahlung is squeezed to smaller polar angles resulting in larger depositions in the inner part of the BeamCal. However, the radial size of the affected area is smaller. Hence, as shown in Fig. 17, the radial range with high electron detection efficiency is larger at $\sqrt{s} = 1$ TeV than at $\sqrt{s} = 500$ GeV.

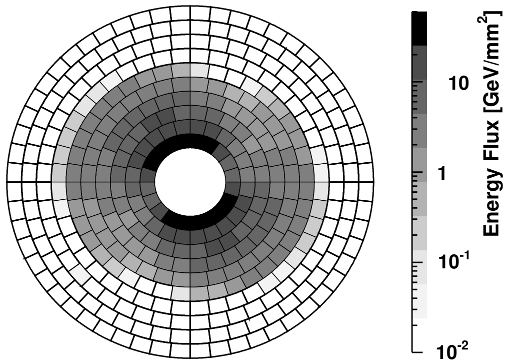

Figure 16: The energy density of beamstrahlung remnants per bunch crossing as a function of the position in the $r - \varphi$ plane. The centre-of-mass energy is 1 TeV. The maximal value of the density is 60 GeV/mm^2.

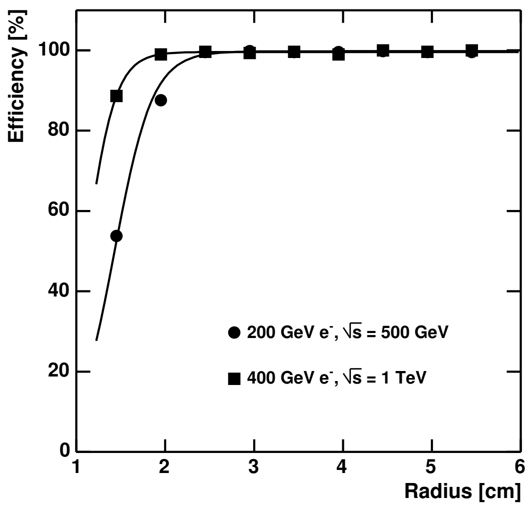

Figure 17: The efficiency to detect a 200 GeV electron on top of background at $\sqrt{s} = 500$ GeV (dots) and a 400 GeV electron on top of background at $\sqrt{s} = 1$ TeV (squares) as a function of the radius at $\varphi \approx 90°$.

4.2.5 The Pile-up Effect

The study of the pile-up effect on the performance of the sandwich calorimeter is done in order to estimate the loss of performance in BeamCal for the 'warm' (normal conducting) accelerator. Pile-up means that depositions from several subsequent bunch crossings are added before they are read-out. This is expected to happen for the warm machine with a designed inter bunch spacing of only 1.4 ns. In the 'cold' machine design the time between two bunch crossings is 337 ns, sufficient to read out the depositions from each bunch crossing separately.

The pile-up effect is studied superimposing the background depositions of 2, 5, 10 and 20 successive bunch crossings. Twenty bunch crossings correspond to the LHC read out timing and is realistic using currently available electronics. The electron detection algorithm is readjusted for each case such that its efficiency is equal to the single bunch crossing case. Then, the fake rate is determined. For each case the minimal radius of the ring is determined outside which the fake rate is less then 1% or 10%. Fig. 18a shows this radius as function of the number of superimposed bunch crossings. A steep rise of the radius is observed up to 10 bunch crossings for $\sqrt{s} = 500$ GeV. At 10 bunch crossings the radius approaches the 'cut off' radius of the beamstrahlung depositions, hence the beamstrahlung-spot is totally blind and pile-up of more bunch crossing does not change the situation. At the $\sqrt{s} = 1$ TeV the result is similar, the saturation happens already after the superposition of 5 bunch crossings, as shown in Fig. 18b. This is due to the more squeezed beamstrahlung remnants distribution.

Alternatively, keeping the fake rate to be less then 1% the electron detection efficiency is studied. This results is a strong performance degradation. The electron detection efficiency approaches zero up to the radius where the saturation in the fake-rate is reached.

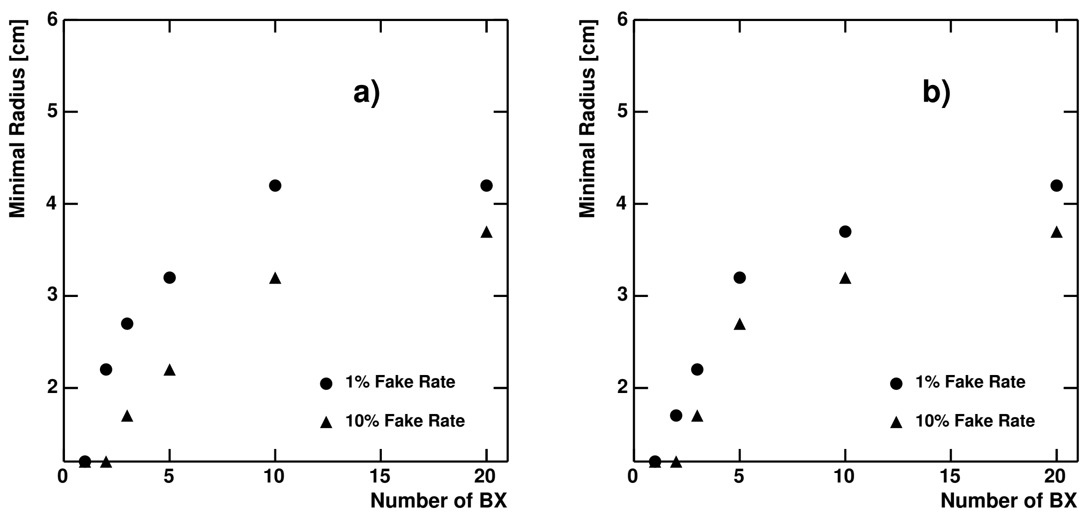

Figure 18: The minimal radius of the ring outside which the fake rate is less then 1% (dots) or 10% (triangles) for a) the $\sqrt{s} = 500$ GeV and b) the $\sqrt{s} = 1$ TeV.

4.3 Beam Diagnostics

The spatial and spectral distributions of the beamstrahlung remnants depend on the beam parameters. Appropriately defined moments of these distributions can be used to monitor and tune the beam. As an example, Fig. 19 shows the variation of the first radial moment of the energy,

$$< \mathrm{R} > = \sum \mathrm{R_i E_i} \; / \; \sum \mathrm{E_i},$$

on the horizontal beam size. The index i runs over all segments, $\mathrm{E_i}$ is the energy deposition and $\mathrm{R_i}$ the radius of the i-th segment[6]. Other quantities used are the azimuthal moment of the energy, the thrust value, and the left-right and top-bottom asymmetries of the deposited energy. A matrix is defined which transforms the values of the beam parameters to the observed quantities. The matrix represents the linear term of a Taylor expansion. The matrix elements are determined from slopes as in the example shown in Fig. 19. Using the measured quantities from a given bunch crossing, the inverse of the matrix is used to calculate the beam parameters. The result of this procedure is listed in Table 2 for several beam parameters. The precision for the determination of each beam parameter in Table 2 is obtained while keeping all other parameters at their nominal values. Several parameters can be determined in parallel at a moderate loss in precision. In addition, all parameters can be determined separately for the electron and positron beams from the calorimeters on opposite sides of the interaction point.

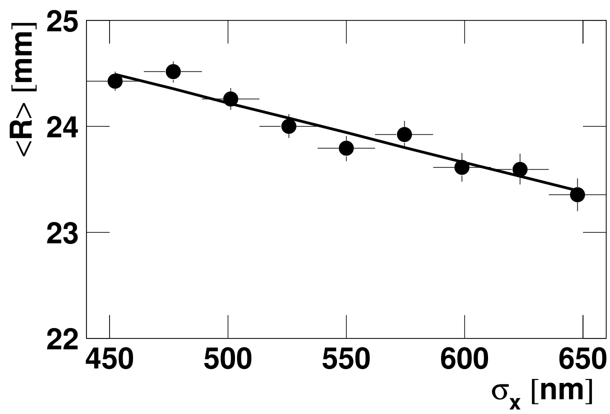

Figure 19: The first radial moment of the beamstrahlung energy as a function of the horizontal beam size σ_x.

The results show the potential of the BeamCal for the determination of beam parameters. Due to the large bunch spacing of TESLA, these measurements can be made within a few bunch crossings and the results can be fed back into the control system of the accelerator.

[6]The distributions used here are obtained summing up the energies deposited on the calorimeter front side with the segmentation as shown in Fig. 11. No shower simulation inside the detector is done.

Table 2: The accuracies reached for several beam parameters from the analysis of the energy depositions in the BeamCal

Quantity	nominal value	precision
bunch width in x	553 nm	1.2 nm
bunch width in y	5.0 nm	0.1 nm
bunch length in z	300μm	4.3μm
beam offset in x	0	7 nm
beam offset in y	0	0.2 nm

5 The PhotoCal

PhotoCal is a proposal for a calorimeter positioned downstream of the interaction region to measure the tails of the beamstrahlung photons. The structure of this calorimeter is similar to the diamond-tungsten sandwich calorimeter shown in Fig. 9. Instead of the diamond sensors, a heavy gas, C_3F_8, is used to measure the deposited energy. The shower particles ionize the gas and the electrons from the ionization are collected by copper pads on a printed circuit board, as shown in Fig. 20. The boards are positioned in the center of

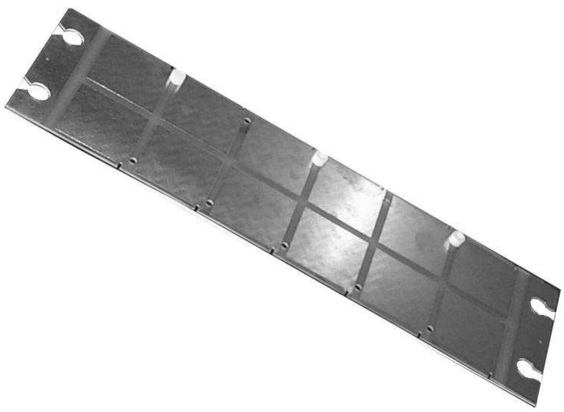

Figure 20: A picture of the printed circuit board with readout pads to collect the ionization electrons in a heavy gas ionization chamber. The size of the pads is 4$\times$4 cm^2.

the gap between two tungsten absorber disks.

The calorimeter covers polar angles between 100 μrad and 400 μrad, catching the angular tails of the beamstrahlungs photons. Azimuthally the calorimeter is subdivided in four sectors and the total deposition in each sector is measured. From the energy deposited in each sector and from left-right and top-bottom asymmetries beam parameters are derived using a neural network. The accuracies obtained are given in Table 3. They are very similar to the ones obtained using e^+ e^- pairs in the BeamCal. However, here additional

Table 3: The accuracies reached for several beam parameters from the analysis of the energy depositions in the Photocal

Quantity	nominal value	precision
bunch width in x	553 nm	4.2 nm
bunch width in y	5.0 nm	0.1 nm
bunch length in z	300μm	7.5μm
beam offset in x	0	4 nm
beam offset in y	0	0.16 nm

measurements are available, and there is hope to improve in the determination of several beam parameters simultaneously using both devices.

6 Sensor Studies

The application of large area diamond sensors for particle detectors is a promising new technology. Studies are done to understand basic features of CVD (Chemical Vapour Deposition) diamond sensors. For a longitudinally segmented heavy element crystal calorimeter a 'proof of principle' is performed. Heavy gas ionization chambers are promising for the application under high radiation doses. Basic performance parameters are studied

6.1 Diamond Sensors

Diamond sensors with an area of about 10×10 mm^2 obtained from three manufacturers are investigated: Fraunhofer Institute for "Angewandte Festkörperphysik" (IAF) in Freiburg, Germany, General Physics Institute Moscow, Russia and Element6, UK. The thickness of the sensors is between 100 μm and 500 μm. The sensors are metallised on both sides with 10 nm Ti and 400 nm Au. For some samples the metallisation is structured on one side in 4 pads of 5×5 mm^2 each. Fig. 21 shows, as an example, an assembled sensor of 12x12 mm^2 size with 4 pads.

As the fist step the dependence of the current on the applied high voltage is measured for all sensors. Only sensors with low leakage currents and a symmetric current vs. voltage characteristic are used for further studies. Most of the sensors show a behavior as shown in Fig. 22. Ramping up the voltage, the currents grow linearly as a function of the voltage. Ramping down the voltage leads to a drop of the current, which may be due to polarization effects in the material. The leakage currents are on the level of 10 pA for an electric field of 1 Vcm^{-1}.

Studies are done of the charge collection efficiency, homogeneity and linearity using minimum-ionizing electrons from a ^{90}Sr source and a hadron beam of about 4 GeV at the CERN PS. The test beam is operated in slow and fast extraction modes. Slow extraction delivers a spill of about one second with low intensities, hence mips can be triggered. The

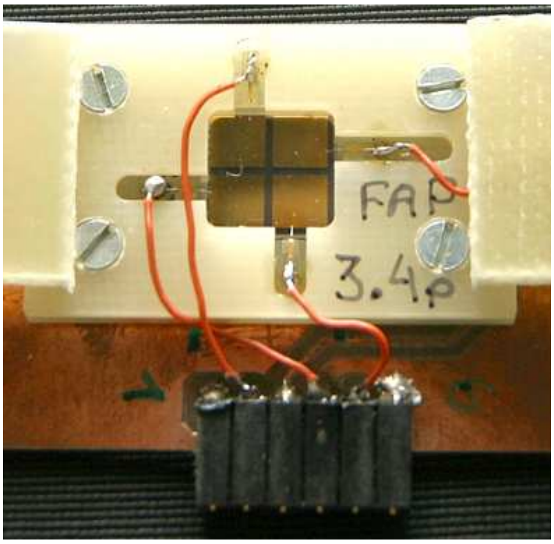

Figure 21: A diamond sensor assembled for test measurements. The metal layer is subdivided into 4 pads, each pad is readout separately.

fast extraction mode delivers a bunch of 10^3–10^6 particles within 10 ns. The test-beam setup is shown in Fig. 23.

The charge measured for a mip passing the sensor as function of the applied electric field is shown in Fig. 24. The ratio between the measured charge and the expected charge calculated from the energy deposited by a mip in the sensor yields the charge collection efficiency. Values between 10% (sensors from IAF) and 40% (sensors from E6) are determined. The sensors from GPI did not show a signal for mips in these measurements.

The charge collection efficiency is also measured as a function of the absorbed dose. The sensor was irradiated with a ^{90}Sr source. The charge collection efficiency, as shown in Fig. 25, is growing by 20% at low doses and reaches saturation at a dose of about 20 Gy. Such a behavior, denoted as priming, was previously observed [29].

To perform homogeneity measurements the position of the diamond sensor is changed with respect to the scintillator position using an XY movable table. The response for mips is stable within a few %.

To test linearity of the diamond sensors the intensity of the beam is changed in the fast extraction mode. The signals of the diamonds are recorded. The signals from the photomultipliers attached to the scintillator are used as reference. Some preliminary results[7] are shown as a scatter-plot in Fig. 26 using the response of the two phototubes and the signal from a diamond sensor and a phototube. A good linearity is observed over a dynamic range of about a factor of 3. A second example is shown in Fig. 27, comparing the signal from two pads on a diamond. Again the signals are nicely proportional to each other. Their

[7]The calibration of the Photo-multipliers for different high-voltage settings and the calibration with respect to an absolute intensity measurement using radio-photoluminescence is not yet finished.

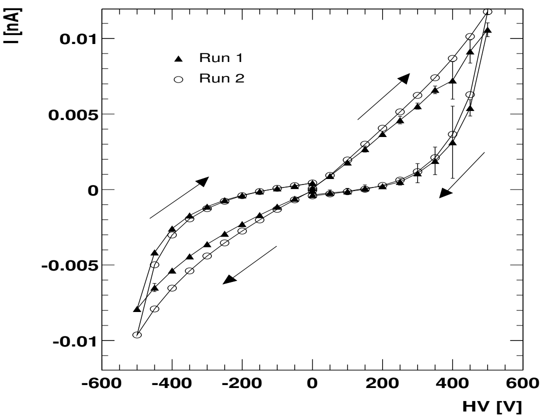

Figure 22: The dependence of the current on the voltage on the two metal-areas of the diamond. The two curves are measurements of the same sensor.

ratio equals unity, supporting also good homogeneity.

After having finished the absolute calibration with respect to the beam intensity we hope to get results on the response of diamond sensors over an intensity range of about 1000.

6.2 Scintillator Segments

In order to demonstrate the feasibility of the light readout concept, as shown in Fig. 10, test segments made from plastic scintillator (Bicron BC-408) are investigated. The light yield and time resolution are measured with photo-multipliers for two setups: the fiber readout discussed here and, for comparison, a direct coupling of the scintillator to the photocathode of the photo-multiplier. The reduction in the light yield is demonstrated in Fig. 28, where the spectra originating from relativistic cosmic muons crossing the scintillator are shown for the direct coupling and for fiber readout. The fiber readout reduces the light yield to 14 % and worsens the time resolution from 1 ns to about 2 ns. These results are promising for the application of this technology to a compact crystal calorimeter with longitudinal segmentation.

6.3 Heavy Gas Ionization Chamber

A heavy gas ionization chamber [30] was operated in an electron beam at the IHEP Protvino with energies between 10 and 40 GeV. The chamber was filled with C_3F_8 and signals are collected from 4x4 cm^2 pads. The number of ionization electrons is shown in Figure 29, summed over all the pads assigned to the electron shower. Good linearity is observed in

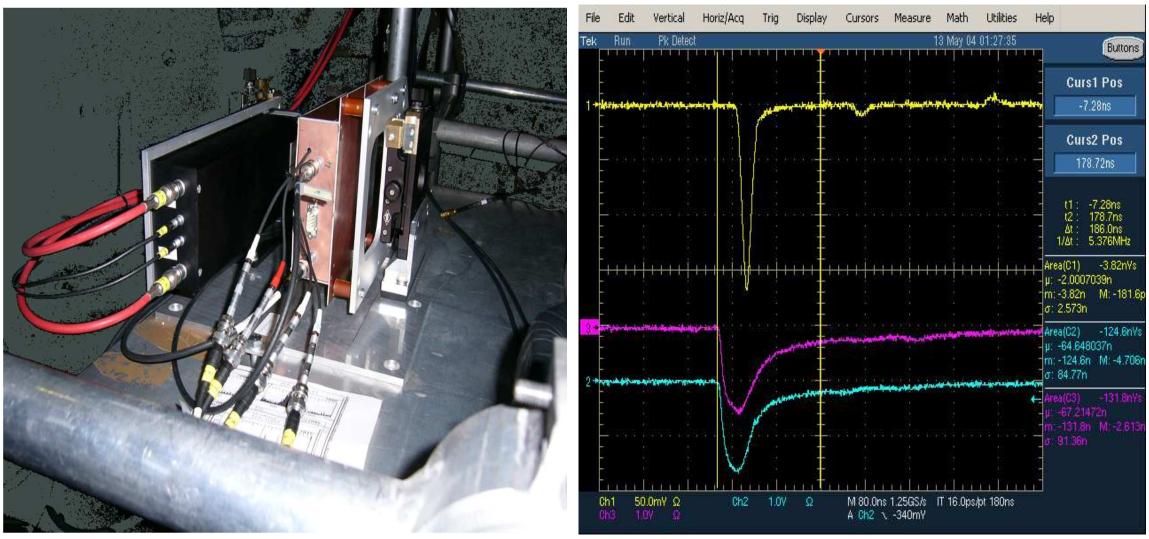

Figure 23: The setup used at the PS at CERN (left). The copper-colored box contains the diamond sensor and a charge sensitive preamplifier for measurements using single particles. The black box is equipped with a 5×5 mm^2 scintillator. Two phototubes are attached to the scintillator, serving as trigger counter or intensity monitor. A typical signal of an IAF diamond in the fast extraction mode (right). The yellow curve is the signal from the diamond, without amplifier. The two other signals stem from two photo-multipliers used as intensity monitor.

the energy range considered. Further tests are planned with smaller pad sizes and to study the linearity over a wider dynamic range.

6.4 Previous Milestones for Sensor Studies for BeamCal

The milestones concerning diamond prototyping are to a large extend matched. However, many effects e.g. concerning the long term behavior of the sensors and irradiation effects are not yet fully understood. Also very large area sensors are not studied so far. Readout electronics is designed for prototype tests. No effort was done for a complex readout system.

The first and second milestone of the heavy element crystal option are matched. The others are postponed. The topic will not be continued at DESY. Other partners have not been found yet.

A heavy gas ionization chamber was tested in the beam. Apart of the aging studies the milestones are considered to be matched. The use of this technology for the proposed PhotoCal needs a reconsideration of the future steps.

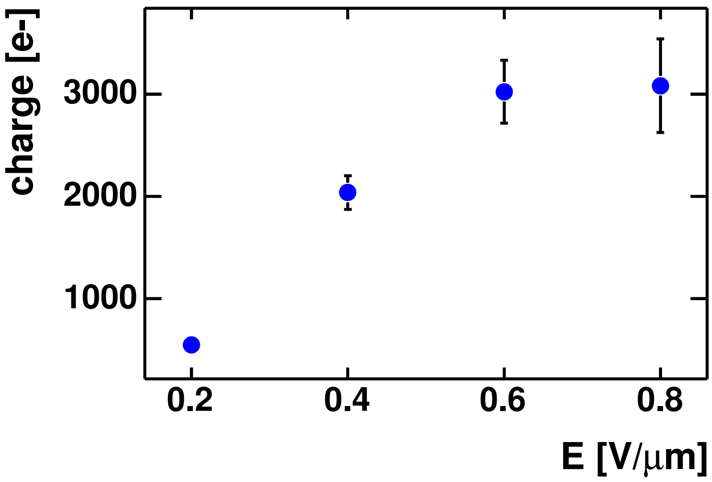

Figure 24: The charge collected in a diamond sensor for a mip as a function of the applied electric field.

7 Milestones for Future R&D

7.1 Milestones for LumiCal

7.1.1 MC Simulations

MC simulations for the LumiCal will be focused on the following topics:

- Performance for a more realistic calorimeter design, including effects of the mechanical frame and a realistic sensor design.
- Detailed comparison of the pad and strip versions. The goal is to make a choice of the more promising version.
- Simulation of the readout electronics and digitization, including noise, cross talk and calibration uncertainties.
- High statistics simulation to define the survey and alignment needs and the number of precision sensor planes.
- Influence of physics background.

These studies will be done within the next 2-3 years. In addition changes of the beam delivery system, e.g. a nonzero crossing angle, have to be faced.

7.1.2 Mechanics Design and Alignment

So far some design work is done to understand the critical points. Now solutions have to be found for the following topics:

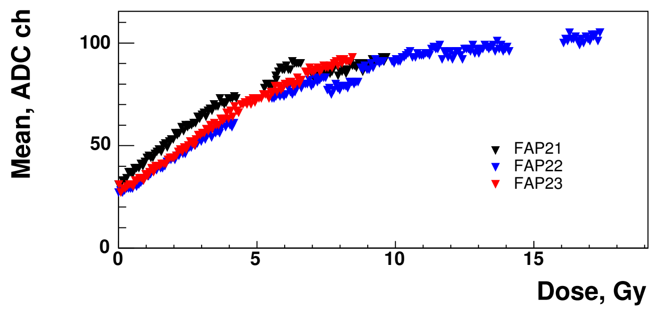

Figure 25: The charge collection efficiency as a function of the absorbed dose for three sensor samples produced by the IAF.

- A detailed design for the mechanical decoupling of the sensor planes from the absorber disks.
- A rough calculation of the deformation of the mechanical structure due to gravitational sag is done for the first version of the design using finite element method. These calculations have to be redone for the decoupled version of the carrier structures and for the ceramic sensor carriers.
- A survey method has to be developed to ensure the accuracy needed for the inner radius. This method has to be tested with a prototype structure.
- Finally a mounting procedure has to be developed, matching the requirements of positioning and alignment.
- Prototyping for a laser alignment system and systematic studies of its performance

We estimate that solutions for the first two items can be found within two years. The latter three items need at least three years of research.

7.1.3 Sensor Prototyping

Based on 4-inch technology a $2{\times}15^\circ$ segment of the calorimeter will be built.

- Thirty layers covering $2{\times}15^\circ$ azimuth angle each and structured in 22 concentric pads will be produced, tested and assembled.
- A prototype of a $2{\times}15^\circ$ calorimeter segment will be built from tungsten and equipped with sensor layers.
- Existing preamplifiers will be tested for the readout of the sensor layers. In case that the tests are not satisfactory a design matching our needs will be done.
- A full system test will done in the lab. If it is successful performance studies in a test-beam at DESY (first stage) and CERN (final stage) are planned.

The first three items will be done within the next 3 years. Depending on the results the measurements in the test-beam will be scheduled.

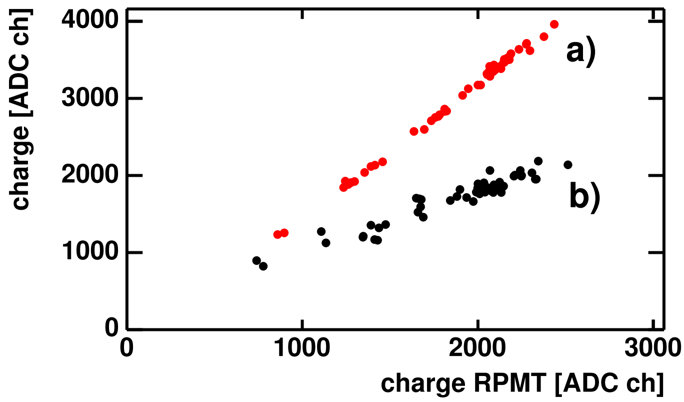

Figure 26: The signal from a diamond (a) and one of the phototubes (b) as a function of the signal from the second phototube.

7.2 Milestones for BeamCal

7.2.1 MC Simulations

So far all simulations are done with an ideal detector. The next steps are:

- Optimization of the segmentation of the detector. The sensor segmentation can certainly be reduced without loosing performance.
- Study of the sensor calibrations using Bhabha events.
- More realistic simulation of the beam diagnostics capabilities.

The effort to be invested here will also depend on possible changes in the beam delivery system. The first two items are planned to be finished within the next two years, the last item is planned for the next three years.

7.2.2 Sensor Prototyping

The studies of general features of diamond sensors will be continued. In collaboration with IAF and other manufacturers larger samples and larger area sensors will be studied. In more detail:

- Completion of the current studies with respect to linearity and homogeneity.
- Deeper understanding of polarization, annealing and priming effects.
- Extension of the studies to larger area sensors to quantify their homogeneity.
- Production of a larger number of sensors to quantify the the stability of the performance (in collaboration with IAF).
- Search for correlations between material features (e.g. photoluminescence spectra) and response for ionizing particles.

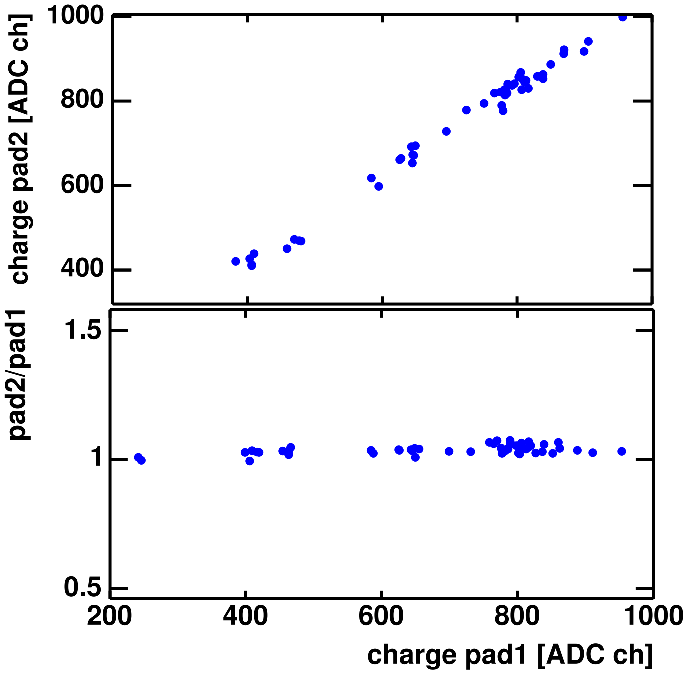

Figure 27: The dependence of the signal from a pad of a structured sensor plotted against the signal of a neighbor pad (top) and their ratio (bottom).

- Study of the sensor performance for large radiation doses.

The study of the first two item will be extended over at least one year, the last four items over three years.

7.2.3 Calorimeter Prototyping

Under the assumption that tests of larger samples and larger area sensors are successful we plan to design and build a prototype of a small calorimeter. Details will be given in two years from now.

7.3 Milestones for PhotoCal

MC simulations have to be done to optimize the shape and the structure of the calorimeter and a procedure has to be developed to combine the informations from BeamCal and PhotoCal to determine beam parameters. The following milestones are set:

- MC simulations for the design of PhotoCal and estimation of the radiation dose.
- Development of an algorithm to determine beam parameters from PhotoCal measurements.

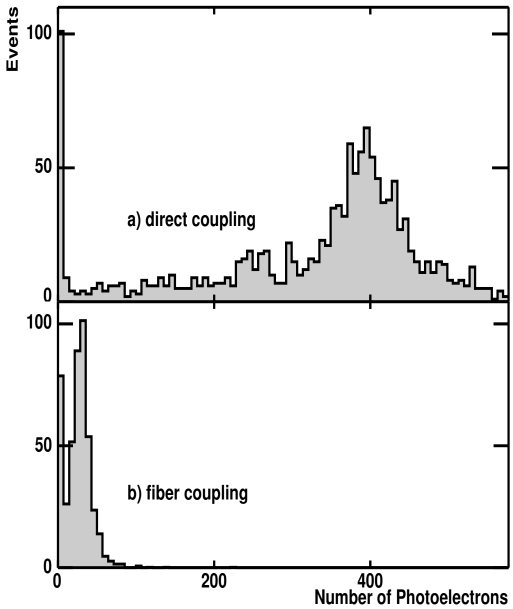

Figure 28: The signal spectra obtained from relativistic cosmic muons for a) the scintillator coupled directly to the photocathode and b) using the fiber readout.

- Understanding of the simultaneous determination of several beam parameters using information from PhotoCal and BeamCal.
- Detailed design of the PhotoCal calorimeter.
- Study of the performance under large radiation doses.

The first two items will be done within 2 years, the last three items within 3 years.

8 Executive Summary

The instrumentation of the very forward region has to face several challenges. A measurement of the luminosity with a precision of $O(10^{-4})$ is mandatory to exploit the physics potential of a linear collider. This precision goal requires calorimeters with sensor positioning accuracy of $O(\mu\mathrm{m})$ at least for a few sensor planes. As a results of a first mechanics design consideration we follow the concept of a decoupling of the support structures for sensor and absorber planes. This concept needs more work in future to investigate its feasibility. Finally tests with a prototype structure will be done to ensure the reach of the benchmarks. A similar challenge is the position monitoring of the installed detector. A test of principle with a laser based system is successfully done. Now a solution applicable for the monitoring of the two calorimeters has to be worked out.

Monte Carlo simulations are done using Bhabha scattering, $e^+e^- \rightarrow e^+e^-(\gamma)$, generators to optimize the shape and segmentation of the calorimeters for the new design of the very

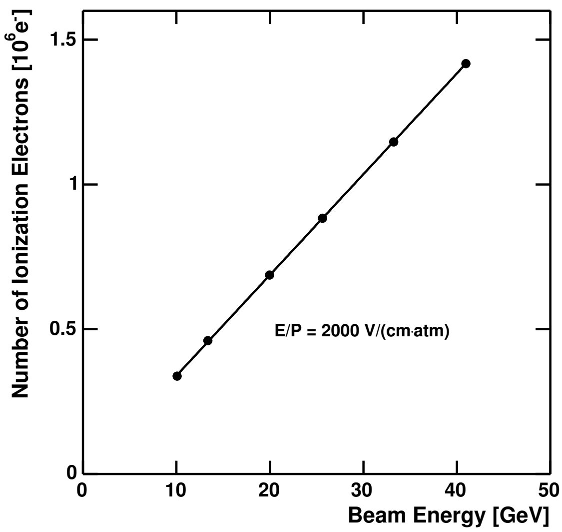

Figure 29: The number of ionization electrons as a function of the electron beam energy.

forward region. At the moment for two versions of the sensor segmentation promising results are obtained. Further studies, including a more realistic treatment of the sensors, must be done to decide which version is superior.

A high statistics simulation is in preparation to identify the best procedure of Bhabha event selection inside the angular interval to be used to measure the luminosity.

The design of the silicon sensors is under preparation. Prototype production and tests are the next steps towards a prototype calorimeter. The test results will also be input for the more realistic Monte Carlo simulations.

The BeamCal extends the coverage of the detector to polar angles of about 5 mrad. At such polar angles beamstrahlung remnants hit the calorimeter resulting in depositions of O(10TeV) per bunch crossing, corresponding to about 10 MGy per year of accelerator operation. Hence radiation hard sensors are needed for this device.

The detection of high energy single electrons at such small angles, necessary to suppress severe background in many search channels, is possible. A compact and fine segmented calorimeter is necessary. The Monte Carlo simulations are done for a diamond-tungsten sandwich calorimeter and a longitudinal subdivided heavy crystal $PbWO_4$ calorimeter with fibre readout. The performance of the sampling calorimeter is found to be superior. It is also shown that the performance of the BeamCal is maintained for a realistic beam simulation and for a centre-of-mass energy of 1 TeV. The fake electron rate is below one per cent for all cases, uncritical for search experiments. However, pile up of the depositions from several bunch crossings will deteriorate the performance strongly.

The BeamCal will also serve for fast beam diagnostics. Monte Carlo simulations have shown that from the distribution of the beamsstrahlung on the calorimeter several beam parameters can be determined with high precision.

We propose to improve the beam diagnostics by a third calorimeter, PhotoCal, which measures the angular tails of the photons originating from beamstrahlung. Also these depositions exhibit a strong dependence on the actual beam parameters.

Further steps to optimize the design of BeamCal are the study of the performance on the sensor segmentation. The hope is to reduce the number of pads without loosing performance. In addition, the impact of Bhabha scattering needs further studies.

Samples of diamond sensors from different manufacturers are tested with a ^{90}Sr source and in the CERN PS beam. The charge collection efficiency of sensors from two manufacturers (E6 and IAP Freiburg) is found to be sufficient for our application. The measurements of linearity and homogeneity, still preliminary and not over the full range or area, are promising. Also the dependence of the charge collection on the absorbed radiation looks reasonable for low doses.

However, several effects about the long term behavior and under irradiation are not yet understood. More studies are needed here. Also the behavior under larger radiation doses must be studied again. More and larger area sensors are needed to quantify the quality.

A prototype segment of a heavy element crystal calorimeter is studied. The segment is subdivided longitudinally into three pieces. Each piece is readout by a fiber guided to the rear end. Light output and cross-talk measurements have shown that this technique can be used to read out a crystal calorimeter with longitudinal subdivision.

A first beam test of a heavy crystal calorimeter is done at the PS in Protvino. Good linearity is observed over a dynamic range of about 4. These studies will be continued to show the feasibility of this device for beamstrahlung photon detection.

9 Miscellaneous

In the last two years we had five collaboration meetings. The talks given there can be found under:
http://www-zeuthen.desy.de/www_users/workshops/lumi/
http://www-zeuthen.desy.de/ astahl/Amsterdam.html
http://www-zeuthen.desy.de/ astahl/Cracow.html
http://www-zeuthen.desy.de/ astahl/Prague.html
http://www-zeuthen.desy.de/lcdet/

In addition, the following talks were given on conferences:

L. Suszycki	Summary of the Very Forward Calorimeter Workshop in Zeuthen, ECFA-
~	DESY Linear Collider Workshop, Prague, November 2002.
K. Kousnetsova	Luminosity and Beam Calorimeter Progress Report, ECFA-DESY Linear
~	Collider Workshop, Amsterdam, April 2003.
V. Drugakov	Simulation of LCAL, ECFA-DESY Linear Collider Workshop, Amster-
~	dam, April 2003.
A. Stahl	New Mask Design, ECFA-DESY Linear Collider Workshop, Amsterdam,
~	April 2003.

W. Lohmann ~	Instrumentation of the Very Forward Region, ECFA-DESY Linear Collider Workshop, Amsterdam, April 2003.
W. Lohmann ~	Overview of Forward Calorimetry R&D and Plans, ECFA-DESY Linear Collider Workshop, Montpellier, November 2003.
K. Afanaciev ~	Results on diamond sensors for the very forward calorimeter, ECFA-DESY Linear Collider Workshop, Montpellier, November 2003.
A. Kowal ~	Optimization of the Design of the Forward Calorimeters, Worlwide Calorimeter Workshop, Montpellier, November 2003.
I. Emelianchik ~	Progress on Forward Calorimetry R&D, Worlwide Calorimeter Workshop, Montpellier, November 2003.
W. Lohmann ~	Summary of Prague workshop on instrumentation in the very forward region, LCWS Paris April 2004.
W. Lohmann (For V. Drugakov) ~	Detection of very forward Bhabha events and electron ID algorithm, LCWS Paris April 2004.
L. Suszycki ~	Experimental Aspects of Precision Luminosity measurement, LCWS Paris April 2004.
L. Zawiejski ~	Review of the forward calorimetry, LCWS Paris April 2004.
R. Ingbir ~	Report on Forward Calorimetry workshop, ECFA Lin. Coll. Workshop, Durham, Sept. 2004.
E. Kouznetsova ~	Diamond sensor testbeam measurements, ECFA Lin. Coll. Workshop, Durham, Sept. 2004.
V. Drugakov ~	Influence of the Pile-Up on the BeamCal Perfomance, ECFA Lin. Coll. Workshop, Durham, Sept. 2004.
R. Ingbir ~	FLC luminosity detector/MC simulations progress report , ECFA Lin. Coll. Workshop, Durham, Sept. 2004.

References

[1] H. Abramowicz et al., *Instrumentation of the Very Forward Region of a Linear Collider Detector*, to appear in IEEE transactions of Nuclear Science, Oct. 2004.

[2] *TESLA Technical Design Report*, DESY 2001-011, ECFA 2001-209, March 2001.

[3] L. Suszycki, talk at the Workshop "'Instrumentation of the Forward Region of a Linear Collider Detector"', 13-14 November 2002, DESY-Zeuthen, Germany http://www-zeuthen.desy.de/www_users/workshops/lumi/.

[4] O. Napoly, Update on $L^* > 3$ m Optics, Talk at the Fourth ECFA/DESY Workshop, Amsterdam, Netherlands, 1-4 April 2003. http://www.nikhef.nl/ecfa-desy/ECspecific/Program/programoverview.htm#APR1st3C.

[5] A. Stahl and K. Buesser, Detector Concept of the Forward Regions, LC Note, to be submitted.

[6] K. Buesser, talk at the Workshop "'Instrumentation of the Forward Region of a Linear Collider Detector"', 26-27 August 2004, DESY-Zeuthen, Germany, http://www-zeuthen.desy.de/lcdet/.

[7] K. Moenig, talk at the Workshop "'Instrumentation of the Forward Region of a Linear Collider Detector"', 26-27 August 2004, DESY-Zeuthen, Germany, http://www-zeuthen.desy.de/lcdet/.

[8] G. Abbiendi et al., The OPAL collab., Eur. Phys. J. C **14**, 373 (2000).

[9] S. Jadach, talk at the Mini-Workshop "'Electroweak Physics Data and the Higgs Mass"', DESY Zeuthen, Germany, February 28 - March 1, 2003.

[10] S. Jadach et al., Comp. Phys. Comm. **102**, 229 (1997)

[11] S. Jadach, Comp. Phys. Comm. **130**, 244 (2000)

[12] A.B. Arbuzov et al., Eur. Phys. J. C **34**, 267 (2004).

[13] T. Riemann, talk at Workshop "'Instrumentation of the Forward Region of a Linear Collider Detector"', 26-27 August 2004, DESY-Zeuthen, Germany, http://www-zeuthen.desy.de/lcdet/; M. Czakon et al., hep-ph/0406203.

[14] R. Bonciani et al., hep-ph/0405275

[15] T. Behnke, G. Blair, M. Elsing, K. Mönig and M. Pohl. *BRAHMS: A Monte Carlo for a Detector at a 500/800 GeV Linear Collider. LC-TOOL-2001-005*, 2001.

[16] R. Brun, F. Bruyant, M. Maire, A.C. McPherson, P. Zanarini, *GEANT3*, Preprint CERN DD/EE/84-1, 1984, revised September 1987.

[17] W. Placzek et al., Phys. Lett. **B390** 298, 1997.

[18] T. Ohl, hep-ph/9607454-rev.

[19] T.C. Awes, F.E. Obenshain, F. Plasil, S. Saini, S.P. Sorensen and G.R. Young, *A simple method of shower localisation and identification in laterally segmented calorimeters*, Nucl. Instrum. and Methods, vol. **A 311**, pp. 130-138, 1977.

[20] A. Stahl, talk at the "'Workshop on Instrumentation of the Very Forward Region"', Amsterdam 2003; http://www-zeuthen.desy.de/ astahl/Amsterdam.html.

[21] W. Wierba, J.Zachorowski and K. Oliwa, Report No 1931/PH, www.ifj.edu.pl/reports/2003html, Institute of Nuclear Physics, Cracow 2003.

[22] P. Bambade et al., *Experimental Implications for a Linear Collider of the SUSY Dark Matter Scenario*, LC Nota, LC-PHSM-2004-016.

[23] D. Bédérède, E. Beuville, B. Bloch-Devaux, L. Gosset, A. Joudon, E. Lançon et *al.*, (ALEPH Collaboration), *SICAL - a high precision silicon-tungsten luminosity calorimeter for ALEPH*, Nucl. Instrum. and Methods, vol. **A 365**, pp. 117-134, 1995; G. Abbiendi K. Ackerstaff, G. Alexander, J. Allison, K.J. Anderson, S. Anderson et *al.* (OPAL Collaboration), *Precision luminosity for Z^0 lineshape measurements with a silicon-tungsten calorimeter*, Eur. Phys. J., vol. **C 14**, pp. 373-425, 2000.

[24] T. Behnke, M. Doucet, N. Ghodbane, A. Imhof, *Radiation Hardness and Linearity Studies of CVD Diamonds*, Nucl.Phys.Proc.Suppl., vol. **125**, pp. 263-266,2003; hep-ex/0212018.

[25] H.M. Araujo, A. Stahl and D.J. Miller, *A lead Tungstate Detector with Integrated Light Readout for the TESLA Luminosity Calorimeter*, LC Note 2001-12-18, http://www-flc.desy.de/lcnotes/.

[26] ILC-TRC Second Report, http://lcdev.kek.jp/TRCII/REPORT.HTM.

[27] D. Schulte. Study of Electromagnetic and Hadronic Background in the Interaction Region of the TESLA Collider. *TESLA 97-08*, 1996.

[28] D. Schulte, N. Walker, G. White, *Intra-Bunch-Train Luminosity Optimisation for the TESLA Linear Collider* DESY-M-03-01R, Proceedings of the 2003 Particle Accelerator Conference, Portland, Oregon, pp. 2733-2736, 2003; G. White, http://hepwww.ph.qmul.ac.uk/lcdata/.

[29] A. Oh, Ph. D. Thesis, Univ. of Hamburg 1999, http://www-library.desy.de/cgi-bin/showprep.pl?desy-thesis-99-022.

[30] V. Bezzubov, S. Denisov, S. Erin, A. Ferapontov, Yu. Gilitzky, V. Korablev et *al.*, *A gas ionization electromagnetic calorimeter filled with* C_3F_8, Nucl. Instrum. and Methods, vol. **A 494**, pp. 369-372, 2002.